Phase Behavior and 3D Structure of Strongly Attractive Microsphere−Nanoparticle Mixtures

James F. Gilchrist,[†] Angel T. Chan,[†] Eric R. Weeks,[‡] and Jennifer A. Lewis*,[†,‖]

Materials Science and Engineering Department and Frederick Seitz Materials Research Laboratory, University of Illinois at Urbana-Champaign, Urbana, Illinois 61801, and Physics Department, Emory University, Atlanta, Georgia 30322

We investigate the phase behavior and 3D structure of strongly attractive mixtures of silica microspheres and polystyrene nanoparticles. These binary mixtures are electrostatically tuned to promote a repulsion between like-charged (microsphere−microsphere and nanoparticle−nanoparticle) species and a strong attraction between oppositely charged (microsphere−nanoparticle) species. Using confocal fluorescence scanning microscopy, we directly observe the 3D structure of colloidal phases assembled from these mixtures as a function of varying composition. In the absence of nanoparticle additions, the charged-stabilized microspheres assemble into a polycrystalline array upon sedimentation. With increasing nanoparticle volume fraction, nanoparticle bridges form between microspheres, inducing their flocculation. At even higher nanoparticle volume fractions, the microspheres become well coated with nanoparticles, leading to their charge reversal and subsequent restabilization. We demonstrate how this fluid−gel−fluid transition can be utilized to control the morphology of the colloidal phases formed under gravity-driven sedimentation.

Introduction

There is a growing interest in controlling the phase behavior, rheology, and structure of colloidal suspensions through nanoparticle additions. The behavior of these binary mixtures is governed by interactions among colloidal, colloid−nanoparticle, and nanoparticle species.[1−18] Recently, Chan and Lewis[16] reported that important differences in system stability emerge in silica microsphere−polystyrene mixtures with electrostatically tuned interactions, depending on whether the added nanoparticles serve as bridging,[1−6] depletant,[9−11] or haloing[12−18] species. When the microsphere−nanoparticle interactions are strongly attractive, heteroflocculation ensues due to nanoparticle bridging.[16] This aggregation mechanism is relevant for many technological applications including the assembly of core−shell composite particles,[19] ceramics,[20] pigments,[21] coatings,[22] and even pharmaceutical materials.[23]

Heteroflocculation of binary mixtures of oppositely charged colloids has been investigated previously, albeit at relatively modest size ratios ($a_{large}/a_{small} \approx 1-15$).[19−30] Early studies focused on determining heteroflocculation kinetics,[3,23−26] characterizing the resulting core−shell composite particle morphology by electron microscopy,[7] and determining compositional effects on their rheological behavior.[31] More recently, light scattering techniques have been applied to quantify the structure of clusters that form during heteroflocculation of like-sized particle mixtures ($a_{large}/a_{small} \approx 1$) of varying charge.[32,33] In such systems, irregular clusters with a lower fractal dimension than that observed during homoaggregation by diffusion-limited cluster aggregation have been reported.[32] Despite recent advances in direct visualization methods, the 3D structural evolution of strongly attractive binary mixtures

† Materials Science and Engineering Department, University of Illinois at Urbana-Champaign.

‡ Emory University.

‖ Frederick Seitz Materials Research Laboratory, University of Illinois at Urbana-Champaign.

(1) Dumont, F.; Ameryckx, G.; Watillon, A. *Colloids Surf.* **1990**, *51*, 171.
(2) Luckham, P. F.; Tadros, T. F.; Hart, C. A.; Vincent, B. *Colloids Surf.* **1980**, *1*, 281.
(3) Hansen F. K.; Matijevic, E. *J. Chem. Soc., Faraday Trans.* **1980**, *76*, 1240.
(4) Furusawa, K.; Anzai, C. *Colloids Surf.* **1992**, *63*, 103.
(5) James, R. O.; Homola, A.; Healy, T. W. *J. Chem. Soc., Faraday Trans.* **1977**, *73*, 1436.
(6) Kitano, H.; Iwai, S.; Ise, N.; Okubo, T. *J. Am. Chem. Soc.* **1987**, *109*, 6641.
(7) Harley, S.; Thompson, D. W.; Vincent, B. *Colloids Surf.* **1992**, *62*, 163.
(8) Islam, A. M.; Chowdhry, B. Z.; Snowden, M. J. *Adv. Colloid Interface Sci.* **1995**, *62*, 109.
(9) Jenkins, P.; Snowden, M. *Adv. Colloid Interface Sci.* **1996**, *68*, 57.
(10) Walz, J. Y.; Sharma, A. *J. Colloid Interface Sci.* **1994**, *168*, 485.
(11) Sharma, A.; Tan, S. N.; Walz, J. Y. *J. Colloid Interface Sci.* **1997**, *190*, 392.
(12) Tohver, V.; Smay, J. E.; Braem, A.; Braun, P. V.; Lewis, J. A. *Proc. Natl. Acad. Sci.* **2001**, *98*, 8950.
(13) Tohver, V.; Chan, A.; Sakurda, O.; Lewis, J. A. *Langmuir* **2001**, *17*, 8414.
(14) Lee, W.; Chan, A.; Bevan, M. A.; Lewis, J. A.; Braun, P. V. *Langmuir* **2004**, 5262.
(15) Martinez, C. J.; Liu, J.; Rhodes, S. K.; Luijten, E.; Weeks, E. R.; Lewis, J. A. *Langmuir*, in press.
(16) Chan, A. T.; Lewis, J. A. *Langmuir* **2005**, *21*, 8576−8579.
(17) Liu, J. W.; Luijten, E. *Phys. Rev. Lett.* **2004**, *93*, 247802.
(18) Wiese, G. R.; Healy, T. W. *J. Colloid Interface Sci.* **1975**, *52*, 458.

(19) Caruso, F.; Caruso, R. A.; Mohwald, H. *Science* **1998**, *282*, 1111.
(20) Konsztowicz, K. J.; Langlois, R. *J. Mater. Sci* **1996**, *31*, 1633.
(21) Taylor, M. L.; Morris, G. E.; Smart, R. S. *J. Colloid Interface Sci.* **2003**, *262*, 81.
(22) Lessa, M. D. M.; Medugno, C. C. *J. Colloid Interface Sci.* **2001**, *239*, 328.
(23) McLaughlin, W. J.; White, J. L.; Hem, S. L. *J. Colloid Interface Sci.* **1993**, *158*, 333.
(24) Imhof, A.;Dhont, J. K. G. *Phys. Rev. Lett.* **1995**, *75*, 1662; *Phys. Rev. E* **1995**, *52*, 6344.
(25) Karanikas, S.; Louis, A. A. *Phys. Rev. Lett.* **2004**, *93*, 248303.
(26) Bleier, A.; Matijevic, E. *J. Colloid Interface Sci.* **1976**, *55*, 510.
(27) James, R. O.; Homola, A.; Healy, T. W. *J. Chem. Soc., Faraday Trans.* **1977**, *73*, 1436.
(28) Kitano, H.; Iwai, S.; Ise, N.; Okubo, T. *J. Am. Chem. Soc.* **1987**, *109*, 6641.
(29) Ryde, N.; Matijevic, E. *J. Chem. Soc., Faraday Trans.* **1994**, *90*, 167.
(30) Sunkel, J. M.; Berg, J. C. *J. Colloid Interface Sci.* **1996**, *179*, 618.
(31) Luckham, P. F.; Tadros, T. F.; Vincent, B. *Colloids Surf.* **1983**, *6*, 101.
(32) Kim, A. Y.; Berg, J. C. *J. Colloid Interface Sci.* **2000**, *229*, 607.
(33) Kim, A. Y.; Hauch, K. D.; Berg, J. C.; Martin, J. E.; Anderson, R. A. *J. Colloid Interface Sci.* **2003**, *260*, 149.

has received little attention. Moreover, none of the prior studies[34–43] have focused on heteroflocculation in binary systems possessing both high charge and size asymmetry.

Here, we systematically explore the 3D structural evolution of colloidal phases assembled from oppositely charged microsphere–nanoparticle mixtures, where $a_{micro}/a_{nano} \approx 60$. While individual suspensions of either type of particle are stable, upon mixing them together heteroflocculation can ensue depending on the number ratio of small to large species, N_{nano}/N_{micro}. At low nanoparticle concentrations, nanoparticle bridges form between microspheres, leading to their flocculation, while at higher concentrations the nanoparticles form a denser coating on the microsphere surfaces, inducing charge reversal and, ultimately, their restabilization. The fluid → gel → fluid phase transitions observed with increasing nanoparticle concentration occur at well-defined values of N_{nano}/N_{micro}. To probe their 3D structure evolution, we utilize confocal microscopy to directly image individual microspheres within colloidal phases assembled from binary mixtures of varying composition in an index-matched solution under gravity-driven sedimentation. This technique has been successfully employed to characterize and quantify the local and long-range structure of a wide array of colloidal assemblies, including colloidal crystals,[34–37] glasses,[38–40] and gels.[41–43] Colloidal phases assembled from fluid regions of the phase diagram are densely packed, whereas those assembled within the gel region are highly open, disordered structures. A comparison is made between their structure and those reported for thermoreversible[41,42] and depletion[43] gels.

Experimental Section

Materials System. Uniform silica microspheres (Geltech, Alachua, FL) serve as the large colloidal species. These microspheres have an average radius, a_{micro}, of 0.590 ± 0.01 μm, as determined from quantitative image analysis carried out on scanning electron microscopy (SEM) photomicrographs (15000× magnification), and a density of 2.25 g/cm³, as determined by helium pycnometry (model AccuPyc 1330, Micrometrics Instrument Corp., Norcross, GA). Fluorescent amidine polystyrene (fAPS) nanoparticles (Interfacial Dynamics Corp., Portland, OR) serve as the small colloidal species. These nanoparticles have a reported average radius, a_{nano}, of 10 nm and a density of 1.055 g/mL. They are supplied in water at a volumetric solids loading of 1.8%. The microspheres exhibit an isoelectric point at pH ≈ 2.5 and a ζ potential of approximately −52 mV at pH 7 (1 mM sodium nitrate), while the nanoparticles exhibit a ζ potential of 95 mV under these same conditions, as measured by microelectrophoresis (ZetaSizer 3000 Malvern Instruments, Northborough, MA) on dilute suspensions ($\phi = 1 \times 10^{-5}$). Note that the ζ potential measurements could not be carried out in the index-matched (glycerol/water) solution due to its high viscosity.

Suspension Preparation. Microsphere–nanoparticle suspensions are prepared by mixing individual silica and fAPS suspensions together. The fAPS suspensions are prepared by adding an appropriate volume of the nanoparticle suspension to deionized water preadjusted with sodium hydroxide (reagent grade, Fisher Scientific) to pH 7.0. The microsphere suspensions are prepared by adding an appropriate volume fraction of SiO₂ microspheres ($\phi_{micro} = 2.5 \times 10^{-3}$ and 5×10^{-2}) to a glycerol/water solution followed by ultrasonication (model 550 sonic dismembrator, Fisher Scientific, Pittsburgh, PA) for 1 min pulsed at a 1 s on/off sequence at 20 kHz. Sodium nitrite salt (0.1 mM NaNO₃) is added to maintain a constant Debye screening length (κ^{-1}) of 9.6 nm at 0.1 mM NaNO₃. Each suspension is then stirred for 0.5 h prior to mixing. The binary suspensions are stirred for 30 s and then transferred to custom sample cells. Their final solution composition corresponds to a glycerol:water ratio of 2.7:1, which is nearly index-matched to the SiO₂ microspheres, as given by the Lorenz–Lorentz[44] index of refraction mixing rule. We note that dye is not added to the solution due to its adsorption onto either the negatively charged microspheres or the positively charged nanoparticles.

Nanoparticle Adsorption. Binary mixtures having $\phi_{micro} = 1 \times 10^{-1}$ and $0 \leq \phi_{nano} \leq 1 \times 10^{-2}$ are prepared in a glycerol/water (2.7:1) solution. After the microspheres fully settle under gravity-driven sedimentation, 300 μL of the supernatant solution is removed for fluorescent intensity analysis. The number of adsorbed nanoparticles per microsphere ($N_{nano,ads}/N_{micro}$) is determined by comparing the measured intensity to the calibration curves measured from standard fAPS solutions. The nanoparticle surface coverage, Γ (mg/m²), is also determined directly from these data.

Colloidal Assembly. Colloidal phases are assembled from dilute binary mixtures of varying composition that undergo gravity-driven sedimentation in custom sample cells. The total suspension volume is 5 mL for $\phi_{micro} = 2.5 \times 10^{-3}$ and 1.5 mL for $\phi_{micro} = 5 \times 10^{-2}$. Each sample cell is fabricated by attaching a glass tube of 10 mm (i.d.) to a glass coverslip using poly(dimethylsiloxane) (PDMS; Sylgard 184, Dow Corning, Midland, MI). Both the tubes and coverslips are cleaned prior to bonding by immersion in a 2.3:1 sulfuric acid (reagent grade, Fisher Scientific)/hydrogen peroxide (30%, Fisher Scientific) solution for 1 h. They are then rinsed repeatedly with deionized water, dried under a nitrogen stream, and bonded to one another using PDMS.

Direct Imaging of Microsphere–Nanoparticle Mixtures. Confocal laser scanning microscopy is used to image the 3D structure of colloidal phases assembled under gravity from binary mixtures of varying composition. The samples are imaged both during assembly and after three weeks of sedimentation by placing them on the stage of an inverted optical microscope (Leica SP2) equipped with Ar and He/Ne laser sources providing both 488 and 633 nm laser lines and a 63×/1.4 NA oil lens. Images are acquired simultaneously by two photomultiplier tubes (PMTs), one used to acquire reflected light from both microspheres and nanoparticles (613–653 nm) and the other to detect light emitted from fluorescent nanoparticles (500 and 540 nm). The samples are scanned in both the x–y and x–z directions, i.e., parallel and perpendicular to the glass substrate, respectively. Three-dimensional volumes of 29 μm × 29 μm × 32 μm are acquired by capturing 2D images with Δz of 0.122 μm between neighboring 2D cross-sections. This procedure independently captures reflected and fluorescent light from each cross-section simultaneously, taking 7–8 min to scan the entire 3D volume. The sedimented sample is essentially at equilibrium and does not evolve during this time. Multiple volumetric regions are scanned per sample, with each volume containing between ~2000 and 9000 particles depending whether it resided in the gel or crystal state.

Image Analysis. The confocal images are analyzed (IDL, Research Systems, Inc.) by filtering the images and locating particle positions in three dimensions.[45,46] To locate microsphere centers, images obtained from both reflected light and light emitted from fluorescent nanoparticles are filtered to subtract the background and to remove noise at high spatial frequencies.

(34) van Blaaderen, A.; Wiltzius, P. *Science* **1995**, *270*, 1177.
(35) van Blaaderen, A.; Wiltzius, P. *Adv. Mater.* **1997**, *9*, 833–835.
(36) de Hoog, E. H. A.; Kegel, W. K.; van Blaaderen, A.; Lekkerkerker, H. N. W. *Phys. Rev. E* **2001**, *64*, 214071.
(37) Gasser, U.; Weeks, E. R.; Schofield, A.; Pusey, P. N.; Weitz, D. A. *Science* **2001**, *292*, 258.
(38) Courtland, R. E.; Weeks, E. R. *J. Phys.: Condens. Matter* **2003**, *15*, 359.
(39) Weeks, E. R.; Crocker, J. C.; Levitt, A. C.; Schofield, A.; Weitz, D. A. *Science* **2000**, *287*, 627.
(40) Weeks, E. R.; Weitz, D. A. *Phys. Rev. Lett.* **2002**, *89*, 957041.
(41) Varadan, P.; Solomon, M. J. *Langmuir* **2003**, *19*, 509.
(42) Varadan, P.; Solomon, M. J. *J. Rheol.* **2003**, *47*, 943.
(43) Dinsmore, A. D.; Weitz, D. A. *J. Phys.: Condens. Matter* **2002**, *14*, 7581.

(44) Taslc, A. Z.; Djordjevic, B. D.; Grozdanlc D. K. *J. Chem. Eng. Data* **1992**, *37*, 310–313.
(45) Crocker, J. C.; Grier, D. G. *J. Colloid Interface Sci.* **1996**, *179*, 298.
(46) Dinsmore, A. D.; Weeks, E. R.; Prasad, V.; Levitt, A. C.; Weitz, D. A. *Appl. Opt.* **2001**, *40*, 4152.
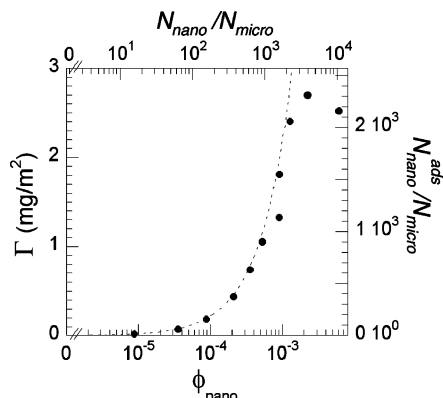
Figure 1. Nanoparticle adsorption as a function of the nanoparticle concentration in solution (expressed by the number ratio of nanoparticles to microspheres, N_{nano}/N_{micro}). The dotted line represents 100% adsorption behavior. The maximum number of adsorbed nanoparticles per microsphere for mixtures with this size asymmetry ($a_{micro}/a_{nano} \approx 60$) is $N_{nano}/N_{micro} = N_{mono}/N_{micro} \approx 2200$.

The fluorescent image is then subtracted from the reflected light image in each 2D slice to remove light reflected from the adsorbed nanoparticles. Each microsphere center is located on the basis of the regional intensity maxima. By averaging the pixel intensity across the microsphere, its location is identified with subpixel accuracy of ∼20 nm in x and y and ∼40 nm in z.[45]

3D reconstructions are obtained for representative sediment structures. The sediment volume fraction, $\phi_{sediment}$, was determined by dividing the total microsphere volume, $V_{micro} = 4N_{tot}/3\pi a_{micro}^3$, where N_{tot} is the total number of microspheres and a_{micro} is the microsphere radius, by the total sampling volume, $26.5 \times 26.5 \times 29.5\ \mu m^3$, and averaging this value over that obtained for multiple scanned regions per sample. The number of nearest neighbors in 3D for each microsphere were found by performing the Delaunay triangulation.[39] The nearest neighbor distributions and Voronoi polyhedron volume distributions are calculated for microspheres away from the volume edges, $22.5 \times 22.5 \times 26\ \mu m^3$. By examining the bond angle and distance between a given microsphere and its nearest neighbors, one can also determine whether a microsphere resides within an amorphous or crystalline structure.[37,47]

Results and Discussion

Nanoparticle Adsorption on Microsphere Surfaces. The adsorption behavior of fluorescent nanoparticles onto silica microspheres from binary mixtures of varying composition is shown in Figure 1. Due to their strong electrostatic attraction to the microsphere surfaces, the nanoparticles fully adsorb from solution until a maximum surface coverage of $N_{nano}/N_{micro} \approx 2200$ is obtained. This corresponds to a packing fraction of ∼0.67 at an effective nanoparticle radius, $a_{nano,eff} \approx 24$ nm.[1,3] Above this nanoparticle concentration, the microsphere surfaces are saturated and excess nanoparticles remain in free in solution.

Phase Behavior of Strongly Attractive Microsphere−Nanoparticle Mixtures. The phase behavior of binary mixtures of varying composition is plotted in Figure 2 in terms of normalized nanoparticle concentration, N_{nano}/N_{micro}. Two distinct phase boundaries are observed at different values of N_{nano}/N_{micro}, as determined by monitoring microsphere sedimentation directly using confocal microscopy. In the absence of nanoparticles, the charged microspheres settle individually to produce either a crystalline or a dense, amorphous sediment at $\phi_{micro} = 2.5 \times 10^{-3}$ and $\phi_{micro} = 5 \times 10^{-2}$. The minimum value of

(47) ten Wolde, P. R.; Ruiz-Montero, MJ.; Frenkel, D. *J. Chem. Phys.* **1996**, *104*, 9932.
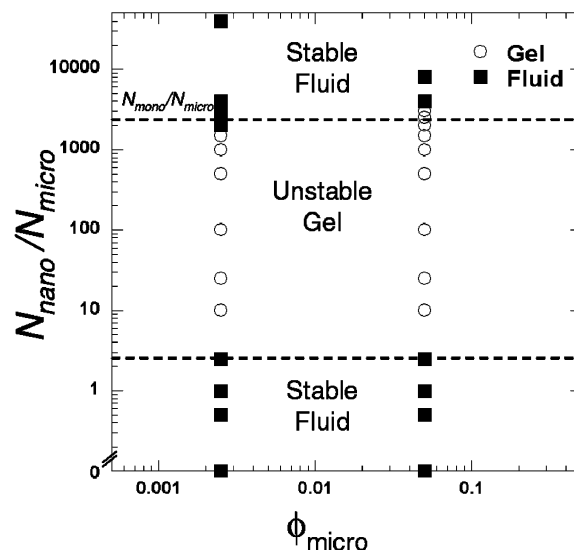

Figure 2. Log−log plot of the phase behavior of microsphere−nanoparticle mixtures. The dashed lines indicate the approximate boundaries between the lower microsphere-charge-stabilized fluid, the nanoparticle-bridging gel, and the upper nanoparticle-charge-stabilized fluid phases.

N_{nano}/N_{micro} expected to induce heteroaggregation is unity, since a single nanoparticle can bridge no more than two microspheres in the high size asymmetry limit.[1] Experimentally, we find that these microsphere−nanoparticle mixtures remain stable at this nanoparticle concentration, with the onset of gelation occurring at higher N_{nano}/N_{micro} values (∼10), similar to previous findings.[2] Higher nanoparticle concentrations are likely required, because the electrostatic repulsion between microspheres may inhibit nanoparticle bridging at lower N_{nano}/N_{micro} values or the distribution of adsorbed nanoparticles per microsphere may be uneven in such mixtures.

At intermediate nanoparticle concentrations (∼10 ≤ $N_{nano}/N_{micro} < N_{mono}/N_{micro}$), nanoparticle bridging leads to microsphere flocculation, with the resulting clusters settling rapidly to form an amorphous sediment that first becomes increasingly more open as N_{nano}/N_{micro} increases and, finally, more compact when N_{nano}/N_{micro} approaches N_{mono}/N_{micro}. Over this concentration range, the sediment is fluorescent while the supernatant is clear, indicating that the nanoparticles fully adsorb onto the microspheres.

At higher nanoparticle concentrations ($N_{nano}/N_{micro} \geq N_{mono}/N_{micro}$), the system is again restabilized, yielding a dense sediment. The microspheres are now well coated with nanoparticles and, hence, stabilized due to a nanoparticle-mediated electrostatic repulsion that results in their charge reversal.[16] The value of N_{mono}/N_{micro} (∼2000) determined from sedimentation exhibits good agreement with the adsorption isotherm measurements shown in Figure 1. Similar to that of samples prepared at intermediate nanoparticle concentrations, the sediment is fluorescent except now the supernatant appears increasingly fluorescent as N_{nano}/N_{micro} increases, since excess nanoparticles remain in solution above N_{mono}/N_{micro}. This restabilizing transition occurs at a slightly higher value of N_{nano}/N_{micro} for mixtures with higher microsphere volume fraction ($\phi_{micro} = 5 \times 10^{-2}$), which may stem from imperfect mixing in these suspensions.

Structure of Colloidal Phases Assembled from Strongly Attractive Microsphere−Nanoparticle Mixtures. The final structure of colloidal phases settled under gravity from index-matched binary mixtures of varying composition is characterized using confocal microscopy.
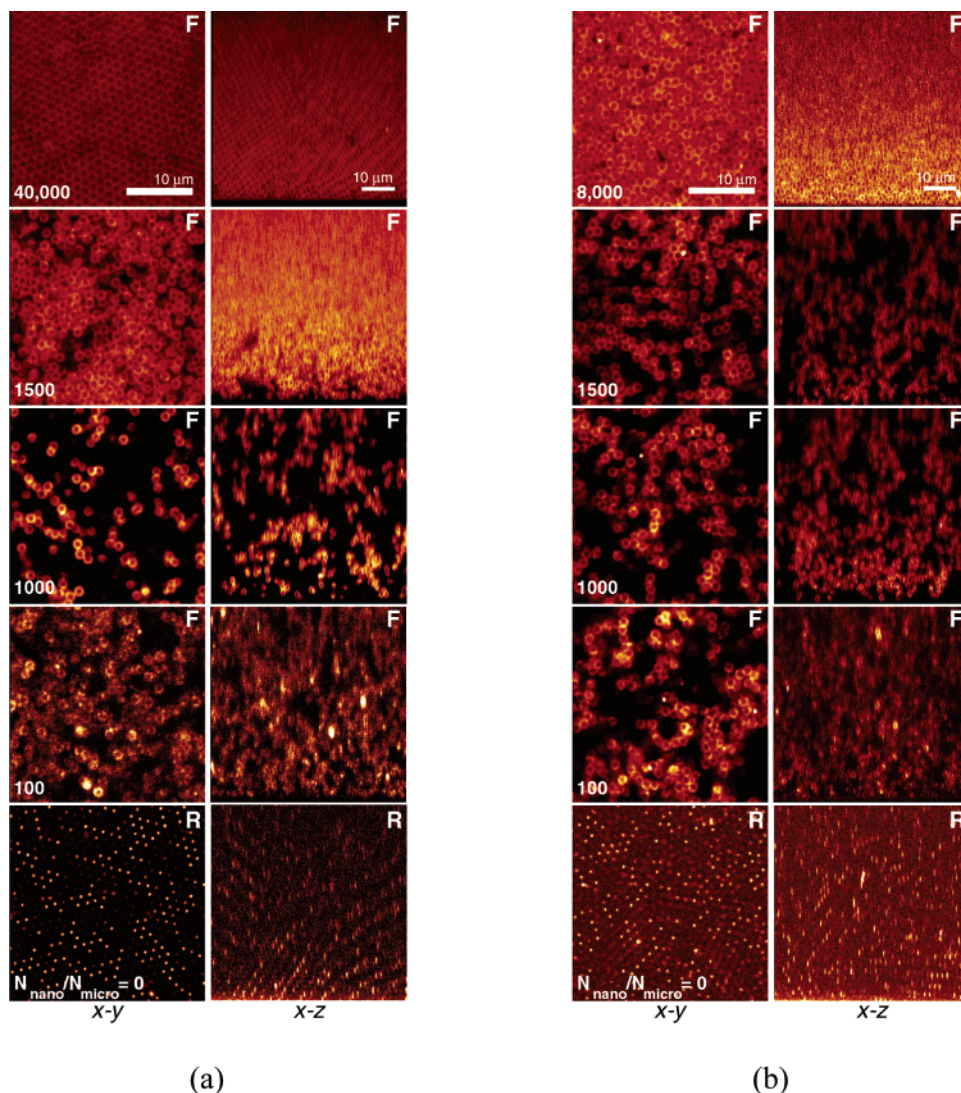
(a)   (b)

Figure 3. Confocal images of the $x-y$ ($z = 5$ μm) and $x-z$ scans (from bottom to top) of sediments formed from binary mixtures of varying composition: (a) $\phi_{micro} = 2.5 \times 10^{-3}$ and (b) $\phi_{micro} = 5 \times 10^{-2}$. [Note: N_{nano}/N_{micro} defines the nanoparticle:microsphere number ratio. Scans denoted "R" and "F" are imaged using reflected ($\lambda = 633$ nm) and fluorescence ($\lambda = 488$ nm) modes, respectively. The scale bars are identical within a given column.]

We report only images acquired on representative samples, shown in Figure 3, although images of all samples measured are included as Supporting Information. In images labeled "R", the brightest features represent light reflected from the individual microspheres. For images acquired on samples of higher nanoparticle concentration, labeled "F", the brightest features are detected fluorescent light. Individual microspheres correspond to dark circular features surrounded by a ring of bright fluorescent nanoparticles adsorbed on their surface, as can be seen in Figure 3. While individual nanoparticles cannot be resolved, local regions with high nanoparticle concentration are clearly evident in these images.

The $x-y$ and $x-z$ scans shown in Figure 3 reveal dramatic differences in the structure of binary mixtures assembled within the three different regions of the phase diagram, where $N_{nano}/N_{micro} = 0$ resides in the lower fluid region, $\sim 10 \leq N_{nano}/N_{micro} < N_{mono}/N_{micro}$ resides in the gel region, and $N_{nano}/N_{micro} \geq N_{mono}/N_{micro}$ resides in the upper fluid region. While these 2D images reveal qualitative trends, we must quantify the 3D sediment volumes, microsphere pair correlation function $g(r)$, distribution of Voronoi polyhedral (VP) volumes, and number of nearest neighbor bonds (NN) per particle for these colloidal phases

to better understand the influence of nanoparticle additions on their structural evolution during gravity-driven sedimentation.

3D reconstructions for representative sections of sediments assembled from these mixtures are shown in Figure 4. Note that data are not provided for samples residing in the lower fluid region, as it was difficult to determine particle centers due to the poor image quality that arises from the lack of fluorescent nanoparticles (see Figure 3). The 3D renderings are color-coded to distinguish colloidal particles in disordered (blue) and crystalline (red) regions. In the unstable (gel) region, the sediments are comprised of open, disordered structures with a minimum sediment density ($\phi_{sediment}$) of ~ 0.1, whereas dense, sometimes polycrystalline structures are observed for samples that settle from binary mixtures that reside in either the lower or upper stable fluid regions (see Figure 5). In these regions, the observed $\phi_{sediment}$ is ~ 0.41 for both bare microspheres and nanoparticle-covered microspheres, indicating that these particles do not behave as hard spheres but have repulsive interactions, and the effective diameter of the charge-stabilized particles is $2a_{micro,eff} \approx 1.30$. This value is in good agreement with the $g(r)$ data reported in Figure 6. The value of N_{nano}/N_{micro} that yields
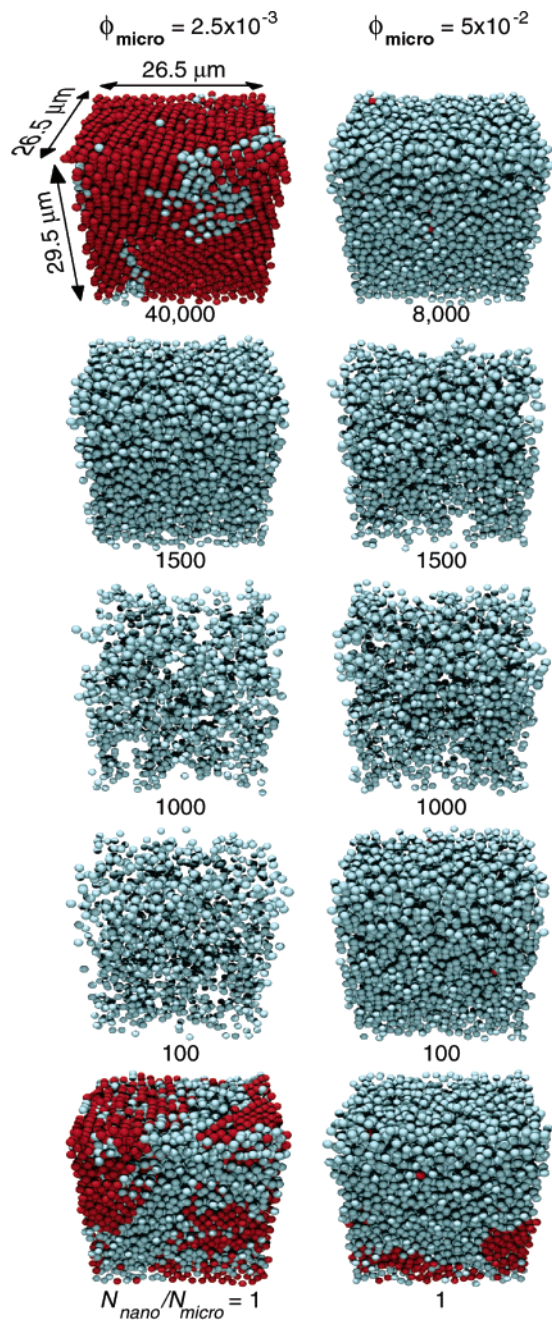
Figure 4. 3D renderings of microsphere locations in sediment structures assembled from binary mixtures composed of varying nanoparticle:microsphere (N_{nano}/N_{micro}) ratios as labeled. Both crystalline and disordered regions are apparent in these images (spheres are drawn to scale).

the most open colloidal gels increases from ~100 for binary mixtures with an initial ϕ_{micro} of 2.5×10^{-3} to ~500 for those with an initial ϕ_{micro} of 5×10^{-2}. Under these conditions, nanoparticle bridging leads to the formation of strong bonds that prohibit significant structural rearrangement during sedimentation.

The microsphere pair correlation functions $g(r)$ of sediments assembled from binary mixtures of varying composition are reported in Figure 6. The peaks in $g(r)$ indicate ordering of particles into coordination shells. The data for crystalline sediments assembled from binary mixtures that reside in the stable fluid phase possess features characteristic of a well-ordered structure; i.e., the particles are organized in multiple coordination shells around a given central particle. The first peak in $g(r)$
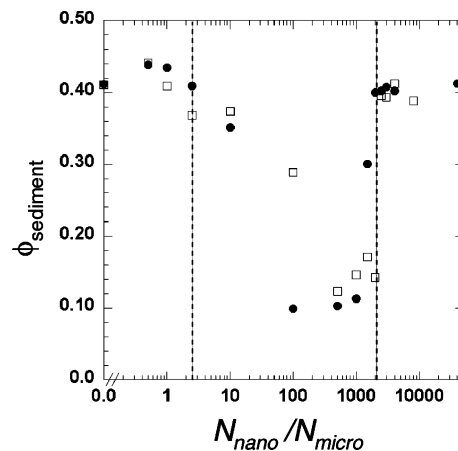

Figure 5. Semilog plot of the sediment volume fraction as a function of the nanoparticle:microsphere number ratio (N_{nano}/N_{micro}) for structures assembled from binary mixtures with (●) $\phi_{micro} = 2.5 \times 10^{-3}$ and (□) $\phi_{micro} = 5 \times 10^{-2}$. The dashed lines denote the phase boundaries indicated in Figure 2. Within the nanoparticle-bridged gel phase, $2.5 < N_{nano}/N_{micro} < 2200$, the volume fraction reaches a minimum of $\phi_{sediment} = 0.11$. In the fluid phase, crystalline and disordered sediments have $\phi_{sediment} \approx 0.41$ due to the large effective microsphere diameters ($2a_{micro,eff} > 1.30 \ \mu m$).
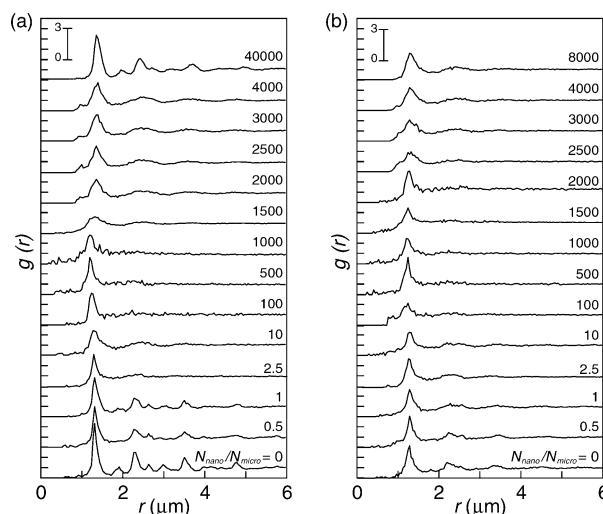

Figure 6. Radial distributions, $g(r)$, acquired on sediment structures assembled from binary mixtures with (a) $\phi_{micro} = 2.5 \times 10^{-3}$ and (b) $\phi_{micro} = 5 \times 10^{-2}$ with varying nanoparticle:microsphere number ratio (N_{nano}/N_{micro}), as specified. Each curve is offset in the vertical direction for clarity.

indicates the distance between nearest neighbors, and in samples without nanoparticles $r = 1.31 \ \mu m$ for neighboring particles in the polycrystalline sediment. As the microsphere volume fraction increases, the degree of order observed for these crystalline sediments lessens considerably for identical N_{nano}/N_{micro} values, as indicated by a significant broadening of the first and higher order peaks. In contrast, the $g(r)$ functions shown for sediments assembled from binary mixtures that reside in the unstable (gel) region of the phase diagram possess features characteristic of a dense liquid structure, such as a broad second peak located at roughly twice the distance of the first peak position. Important differences in their heterogeneity as a function of increasing N_{nano}/N_{micro} (see Figures 3 and 4) only emerge upon further analysis of their structure both locally and longer range through the distribution of NN and Voronoi tessellation.
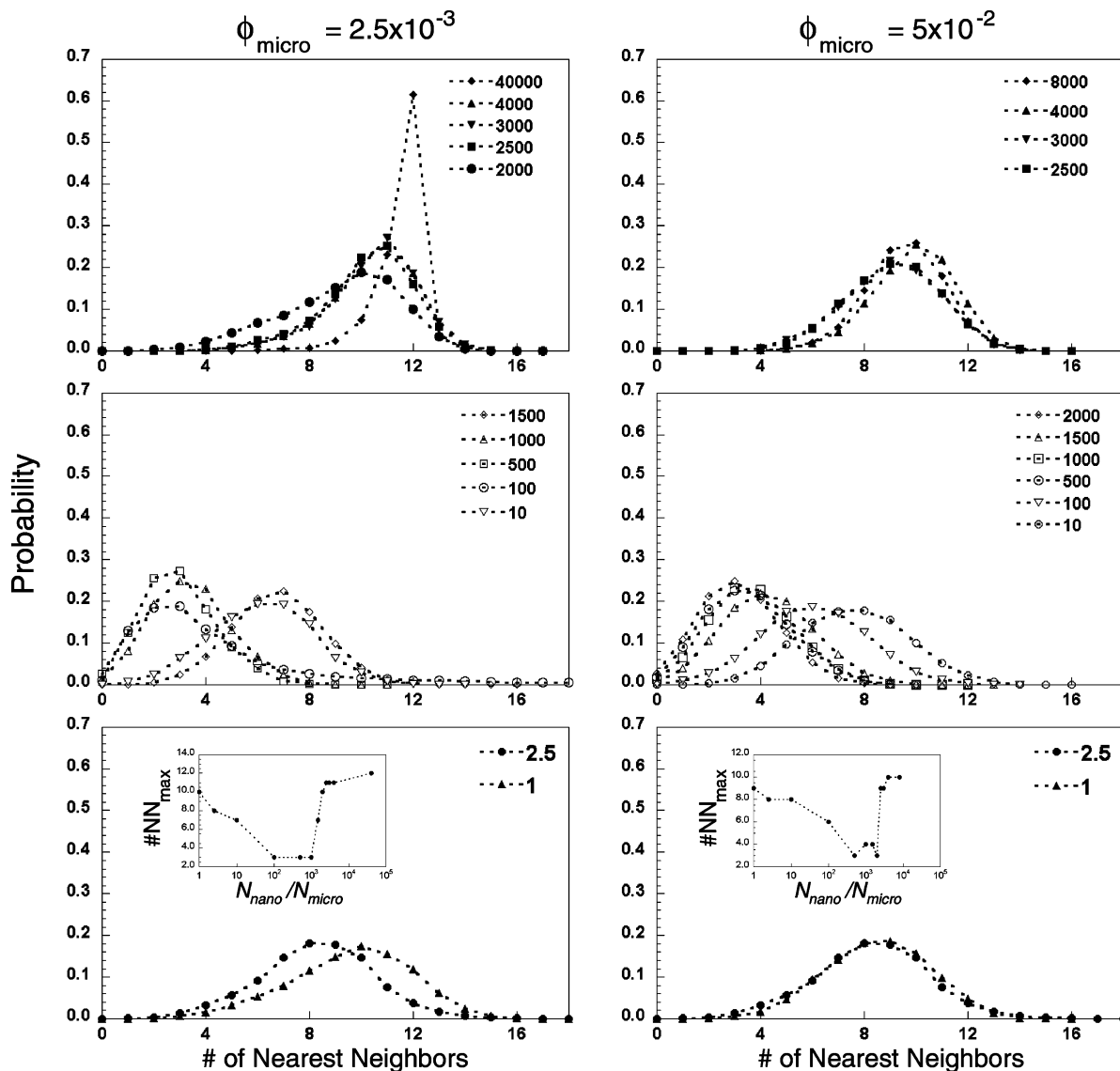
Figure 7. Probability distribution of nearest neighbors for sediment structures assembled from binary mixtures with (left) ϕ_{micro} = 2.5 × 10^{-3} and (right) ϕ_{micro} = 5 × 10^{-2} with varying nanoparticle:microsphere number ratio, N_{nano}/N_{micro}, as specified. [Note: These plots are divided to show the trends associated with each region of the phase diagram (see Figure 2). Insets show the maximum for each curve.]

The NN per particle is depicted in Figure 7 for sediments assembled from binary mixtures of varying composition. This quantity provides insight into the degree of structural rearrangement at the local scale.[42] For a perfect close-packed crystalline sediment, an NN of 12 is expected for every particle, whereas a polycrystalline sample will have a narrow distribution of NN with a peak value of 12 due to domain boundaries between individual crystalline regions. In great contrast, the local topology of strong colloidal gels comprised of rigid, irreversible bonds should be dominated by chainlike aggregates (NN = 2). If particles within a given cluster can rearrange by, for example, rotation, then significant compaction and reorganization can occur, increasing the peak value of NN.

The NN distributions in the lower and the upper fluid regions are broad with a peak NN value above 8, suggesting that microspheres reside in dense sediment. A narrow NN distribution with a peak value of 12 is only observed for binary mixtures assembled from ϕ_{micro} = 2.5 × 10^{-3} at N_{nano}/N_{micro} = 40000. In the unstable region, a marked decrease in the peak NN value is observed, with a minimum of ~3 found for these mixtures. This suggests that the nanoparticle bridges formed between neighboring

microspheres are nearly rigid, irreversible bonds. Similar observations have been reported previously for strong gels.[42,43] Not surprisingly, the strongest microsphere−nanoparticle gels reside deep within the unstable gel phase.[43]

van Blaaderen and Wiltzius[34] and Varadan and Solomon[41] were the first to apply Voronoi tessellation to spatially characterize the respective structures of colloidal glasses and dense colloidal gels, respectively. The standard deviation σ and skewness of the Voronoi polyhedral volume (V_{VP}) distribution are indicative of the structural heterogeneity of the colloidal microspheres within the sediment structures, as shown in Figure 8. The V_{VP} distributions for ϕ_{micro} = 2.5 × 10^{-3} and 5 × 10^{-2} are roughly subdivided into the lower fluid region, the unstable (nanoparticle-bridging) region, and the upper (nanoparticle-restabilized) region for easier comparison of V_{VP} distributions within each phase. In both the lower and upper fluid regions, the V_{VP} distribution is sharply peaked; however, its value of ~2.5 μm^3 is much larger than the theoretical minimum of V_{VP} = 1.16 μm^3, an fcc colloidal crystal assembled from microspheres of a_{micro} = 0.59 μm. Standard deviation in the lower fluid in samples near the fluid−gel phase
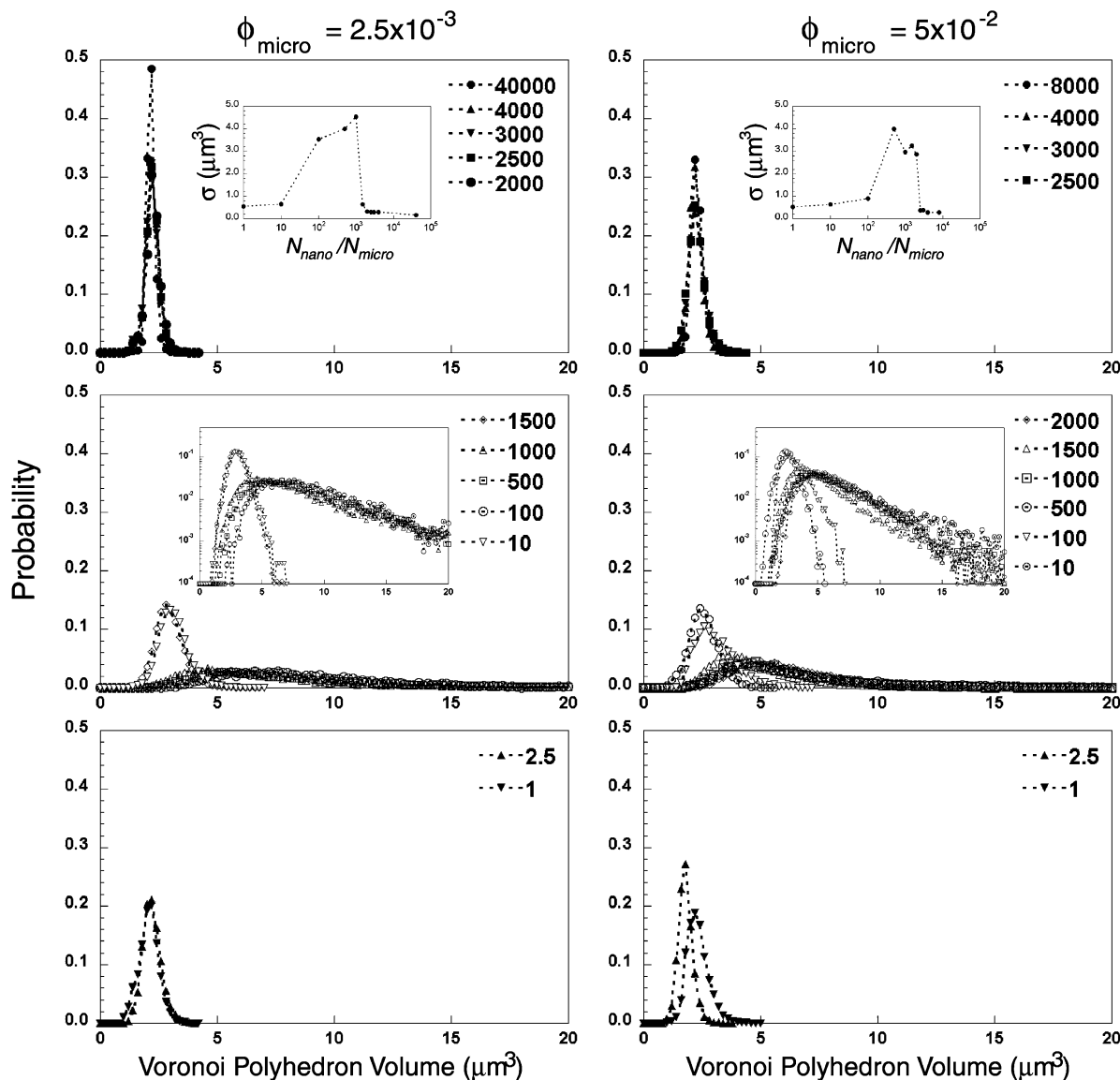
Figure 8. Probability distribution of dimensionless Voronoi polyhedral volumes for sediments assembled from binary mixtures with (left) $\phi_{micro} = 2.5 \times 10^{-3}$ and (right) $\phi_{micro} = 5 \times 10^{-2}$ with varying nanoparticle:microsphere number ratio, N_{nano}/N_{micro}, as specified. [Note: The top insets show the standard deviation (σ) of the data as a function of N_{nano}/N_{micro}, while the middle insets show the log-linear dependence of the distribution in the nanoparticle-bridging gels. These plots are divided to show the trends associated with each region of the phase diagram (see Figure 2).]

boundary is $\sigma \approx 0.5~\mu m^3$ in the lower fluid region. In the upper fluid region, the standard deviation is $\sigma \approx 0.28~\mu m^3$ for samples closer to the phase boundary, decreasing to $\sigma \approx 0.17~\mu m^3$ for the polycrystalline sample found at $N_{nano}/N_{micro} = 40000$. These standard deviations are larger than in binary systems exhibiting stabilization via "haloing".[15]

The most striking features are the linear tails observed in log-linear insets in Figure 8 at larger values of the Voronoi polyhedral volume ($V_{VP} > 6~\mu m^3$) for colloidal gels assembled from binary mixtures that reside in the unstable region of the phase diagram. As seen in the insets in Figure 8, these tails are linear for $V_{VP} > 6~\mu m^3$. Although these reported V_{VP} values are large, the distributions are mostly unaffected by edge effects. This is verified by obtaining similar results for calculations in a subvolume for microspheres farther from the edges of the scanned volume. Varadan and Solomon also found log-linear tails in the V_{VP} distributions[42] and found they collapse onto a universal curve at higher volume fractions when scaled by standard deviation unlike strong gels of lower volume fraction.[41] The σ values for both ϕ_{micro} values investigated

exceed $4.0~\mu m^3$ and relative to the microsphere diameter indicate a degree of heterogeneity unseen in previous studies.[15,41,42] We observe for $\phi_{micro} = 2.5 \times 10^{-3}$ that tails of the V_{VP} distribution of the lowest volume fraction microsphere gel sediments exhibit exponential decay, $P(V_{VP}) \approx \exp(-V_{VP}/V_0)$, with $V_0 \approx 9~\mu m^3$ for $100 \leq N_{nano}/N_{micro} \leq 1500$. At $\phi_{micro} = 5 \times 10^{-2}$, the decay constant decreases from $V_0 \approx 8~\mu m^3$ for $N_{nano}/N_{micro} = 500$ to $V_0 \approx 5~\mu m^3$ for $N_{nano}/N_{micro} = 2000$. The high VP volume values ($V_{VP} > 6~\mu m^3$) observed in the log-linear tails no longer represent local structure surrounding individual particles, but may suggest long-range self-similarity in the microsphere−nanoparticle gels.

Conclusions

The phase behavior and 3D structure of colloidal phases assembled from strongly attractive microsphere−nanoparticle mixtures that possess high charge and size asymmetry have been investigated. The lower phase boundary between the microsphere-charge-stabilized fluid region and the nanoparticle-bridging gel occurs above

$N_{nano}/N_{micro} = 1$, the theoretical minimum for the onset of gelation, likely due to mixing effects. The upper phase boundary between the gel and fluid phases occurs at or above the nanoparticle concentration necessary for monolayer coverage of the microsphere surfaces. Through compositional tailoring, we can selectively tune 3D structure within each of these phases. Novel structures ranging from highly open gels to well-dispersed core−

shell particles were created that may find application in drug delivery,[48] photonic materials,[49] heterogeneous catalysis,[50] and surface-enhanced Raman scatterning.[51]

Supporting Information Available: Confocal microscopy images of all samples measured. This material is available free of charge via the Internet at http://pubs.acs.org.

LA051998K

(48) Langer, R. *Science* **1990**, *249*, 1527.
(49) Rogach, A.; Susha, A.; Caruso, F.; Sukhorukov, G.; Kornowski, A.; Kershaw, S.; Mohwald, H.; Eychmuller, A.; Weller, H. *Adv. Mater.* **2000**, *12*, 333.
(50) Chen, C. W.; Serizawa, T.; Akashi, M. *Chem. Mater.* **1999**, *11*, 1381.
(51) Oldenburg, S. J.; Westcott, S. L.; Averitt, R. D.; Halas, N. J. *J. Chem. Phys.* **1999**, *111*, 4729.